940 *Macromolecules* **2011**, *44*, 940–949
DOI: 10.1021/ma102435a

Macromolecules
ARTICLE

Ionic Conductivity, Capacitance, and Viscoelastic Properties of Block Copolymer-Based Ion Gels

Sipei Zhang,[†] Keun Hyung Lee,[†] C. Daniel Frisbie,*[,†] and Timothy P. Lodge*[,†,§]

[†]*Department of Chemical Engineering and Materials Science, University of Minnesota, Minneapolis, Minnesota 55455, United States, and* [§]*Department of Chemistry, University of Minnesota, Minneapolis, Minnesota 55455, United States*

Received October 25, 2010; Revised Manuscript Received December 29, 2010

ABSTRACT: The effects of composition, temperature, and polymer identity on the electrical and viscoelastic properties of block copolymer-based ion gels were investigated. Ion gels were prepared through the self-assembly of poly(styrene-*b*-ethylene oxide-*b*-styrene) (SOS) and poly(styrene-*b*-methyl methacrylate-*b*-styrene) (SMS) triblock copolymers in a room-temperature ionic liquid, 1-ethyl-3-methylimidazolium bis(trifluoromethylsufonyl)imide ([EMI][TFSI]). The styrene end-blocks associate into micelles, whereas the ethylene oxide and methyl methacrylate midblocks are well-solvated by this ionic liquid. The properties of the ion gels were examined over the composition range of 10−50 wt % polymer and temperature range of 25−160 and 25−200 °C for the SOS- and SMS-based gels, respectively. The response of the ion gels to ac electric fields below 1 MHz can be represented by a resistor and constant phase element (CPE) series circuit, with a characteristic time corresponding to the establishment of stable electrical double layers (EDLs) at the gel/electrode interfaces. The ionic conductivity and specific capacitance were found to range from 3×10^{-5} to 3×10^{-2} S/cm and 0.3 to 10 μF/cm^2, respectively. For 1 mm thick gels, the corresponding *RC* time constants ranged from 2×10^{-5} to 5×10^{-3} s. Notably, at high polymer concentrations, the ionic conductivity is much higher in SOS than SMS due to the higher glass transition of the methyl methacrylate block. Two relaxation modes have been observed in the ion gels under oscillatory mechanical shear. The faster mode corresponds to the relaxation of the midblocks in the ionic liquid, while the slow mode reflects motion of the end-blocks within their micellar cores. The plateau modulus of the gels was found to vary from 0.5 to 100 kPa over the measured composition and temperature ranges. While the ionic conductivity generally decreases as the modulus increases, it is possible to achieve conductivities greater than 0.01 S/cm with moduli above 10 kPa in the SOS system.

Introduction

Ionic liquids have generated considerable research interest over the past decade as a promising class of materials for a number of applications.[1−6] Their unique combination of physicochemical properties,[7] such as negligible vapor pressure, nonflammability, exceptional chemical, thermal, and electrochemical stability, optical transparency, and high ionic conductivity, makes ionic liquids exceptional electrolytes for electrochemical devices.[4−6] The relatively weak electrostatic interactions between component ions and the very high ionic concentration ($\sim 10^{21}$ cm^{-3} at room temperature)[8] enable facile response of ionic liquids to external electric fields, and hence they have much higher ionic conductivity than conventional polymer electrolytes utilizing lithium salts, e.g., PEO/$LiClO_4$ ($\sim 10^{-5}$ S/cm at room temperature).[9] In addition, the large numbers of component ions and their possible combinations offer enormous flexibility in materials design.

The mechanical integrity that ionic liquids lack can be supplied by mixing them with low molecular weight gelators[10,11] or more often macromolecules,[12,13] forming what is referred to as an ion gel. With the combined properties of ionic liquids and a persistent structure, ion gels have gained popularity as novel functional materials that exhibit the potential to be utilized in a variety of applications including gas separation,[14] lithium batteries,[15,16] electromechanical actuators,[17,18] and organic thin-film transistors.[19−24]

*To whom correspondence should be addressed. E-mail: frisbie@umn.edu (C.D.F.); lodge@umn.edu (T.P.L.).

Ion gels based on polymer/ionic liquid composites are generally prepared by chemically or physically cross-linking polymeric networks in ionic liquids. Chemical cross-linking can be realized through polymerization of vinyl monomers in the presence of a cross-linker,[25,26] the polyaddition reaction of monomers with multifunctional reactive groups,[27−30] or both.[31] Alternatively, physical cross-linking can be achieved by the self-assembly of ABA triblock copolymers, where the A block is insoluble in the ionic liquid.[32−36] Monomers, block lengths, block sequence, and copolymer content can be varied to obtain desired structures and properties, thus offering practically unlimited tunability when combined with the selection of ionic liquids.

Polymeric ion gels are among the most conductive solid polymer electrolytes due to the high ionic conductivity of ionic liquids.[37] Mechanical integrity is also an important figure of merit for electrochemical applications of ion gels. However, the relatively few publications that report these properties tend to focus on conductivity rather than modulus. For instance, in their pioneering work on chemically cross-linked ion gels, Watanabe and co-workers measured the ionic conductivity of gels formed by *in situ* radical polymerization of methyl methacrylate (MMA) in the ionic liquid 1-ethyl-3-methylimidazolium bis(trifluoromethylsufonyl)imide ([EMI][TFSI]) over the whole composition range at varied temperatures.[25] With regard to mechanical properties, however, the authors only confirmed the gels to be self-standing, and no direct measure of gel strength was performed. More recently, we have developed physically cross-linked ion gels formed by the self-assembly of poly(styrene-*b*-ethylene oxide-*b*-styrene)

 Published on Web 01/19/2011

Table 1. Molecular Characterization of SOS and SMS Triblock Copolymers and PEG and PMMA Homopolymers

polymer	code	$M_{n,PS}$ (kDa)[a]	$M_{n,PMMA}$ (kDa)	$M_{n,PEO}$ (kDa)	PDI
PS−PEO−PS	SOS(3−35−3)	2.8		35	1.03
PS−PMMA−PS	SMS(18−86−18)	17.5	86		1.21
PEG				35	1.04
PMMA	PMMA(86)[b]		86		1.20
	PMMA(126)[c]		126		1.07

[a] Block M_n determined by NMR. [b] Macroinitiator used to synthesize SMS. [c] Sample used to prepare homopolymer solutions. This polymer was previously synthesized by Zeroni[44] using anionic polymerization.

(PS−PEO−PS) in the ionic liquid 1-butyl-3-methylimidazolium hexafluorophosphate ([BMI][PF_6]), where the PS blocks are insoluble and the PEO block is compatible with the ionic liquid.[32] The storage modulus of gels containing 4−10 wt % polymer was found to be ~1 kPa, while ionic conductivities not much lowered from the bulk ionic liquid were observed for gels with 5 and 10 wt % polymer. We further reported thermoreversible ion gels by the self-assembly of poly(*N*-isopropylacrylamide-*b*-ethylene oxide-*b*-*N*-isopropylacrylamide) in [EMI][TFSI] and measured both ionic conductivity and modulus of the gel with 10 wt % polymer.[33] However, these two studies only focused on ionic conductivity at one or two compositions. More systematic studies of both mechanical and electrical properties of ion gels are desirable.

To this end we examine the response of block copolymer-based ion gels formed by the self-assembly of PS−PEO−PS and poly(styrene-*b*-methyl methacrylate-*b*-styrene) (PS−PMMA−PS) in [EMI][TFSI], to both oscillatory electric fields and mechanical shear strains in the ionic-liquid-rich composition regime over wide temperature ranges. Important parameters including ionic conductivity, specific capacitance, *RC* time constant, and the plateau modulus of the gels were determined. [EMI][TFSI] was chosen because it has been widely used in electrochemical applications due to its stability, low viscosity, and large electrochemical window. The PS−PEO−PS and PS−PMMA−PS block copolymers were used due to the well-known solubility of the midblocks in [EMI][TFSI] and the distinct difference in the glass transition of the midblocks ($T_{g,PEO} \sim -60$ °C, $T_{g,PMMA} \sim 110$ °C).[38] The overall goal is to understand the ionic and viscoelastic motions in these ion gels to enable rational design of high-performance microstructured electrolyte materials.

Experimental Section

Polymer Synthesis and Characterization. All reagents were used as received unless otherwise noted. The PS−PEO−PS triblock copolymer was synthesized via reversible addition−fragmentation chain transfer polymerization (RAFT) from a poly(ethylene glycol) (PEG) precursor following a previously reported procedure.[34] The chain transfer agent (CTA), (*S*)-1-dodecyl-(*S*′)-(α,α′-dimethyl-α′′-acetic acid) trithiocarbonate, synthesized following a reported protocol,[39] was coupled to the PEG precursor via an acid chloride intermediate. The PS end-blocks were subsequently grown on the CTA end-capped PEO macroinitiator. The PS−PMMA−PS triblock copolymer was synthesized by a two-step atom transfer radical polymerization (ATRP).[40−43] CuBr and $CuBr_2$ were stored in the glovebox to avoid water absorption. MMA and styrene monomers were passed through active alumina columns prior to use. In the first step, a difunctional PMMA macroinitiator was prepared. The initiator diethyl *meso*-2,5-dibromoadipate (0.253 g, 7.0×10^{-4} mol) and $CuBr_2$ (0.008 g, 3.6×10^{-5} mol) were mixed with 80 mL of anisole and stirred at 60 °C to ensure complete dissolution, followed by cooling to room temperature and then with an ice bath. MMA (120 mL, 1.12 mol), *N*,*N*,*N*′,*N*′′,*N*′′-pentamethyldiethylenetriamine (0.095 mL, 4.6×10^{-4} mol), and CuBr (0.051 g, 3.6×10^{-4} mol) were then added and dissolved. The solution was freeze−pump−thaw degassed for three cycles, and polymerization was carried out at 60 °C for 6 h. The contents were poured into 5 L of methanol and stirred vigorously to remove most of the copper, and the resulting precipitate was dissolved in ethyl acetate. The solution was then passed through a neutral alumina column and reprecipitated in *n*-hexane. The product was dried in a vacuum oven for a day. In the second step, the PMMA macroinitiator (28.0 g, 0.28 mol), mixed powder of CuBr and $CuBr_2$ (97:3 in mole, 0.182 g, 1.25×10^{-3} mol), and 4,4′-dinonyl-2,2′-bipyridine (1.067 g, 2.61×10^{-3} mol) were dissolved in styrene (80 mL, 0.7 mol). The solution was degassed via five freeze−pump−thaw cycles, after which polymerization was carried out for 64 h at 100 °C. Purification was the same as in the first step, with an additional reprecipitation in cyclohexane to remove PS homopolymer. The final product was dried at room temperature in a vacuum oven for 2 days.

The product of each reaction step was confirmed by ^{1}H NMR spectroscopy and characterized by size exclusion chromatography (SEC). Table 1 lists the molecular weight of each block and the overall polydispersity (PDI) of all polymers investigated. For simplicity, the PS−PEO−PS and PS−PMMA−PS triblock copolymers are denoted as SOS(3−35−3) and SMS(18−86−18), respectively.

Ionic Liquid, Polymer Solution, and Ion Gel Preparation. The [EMI][TFSI] ionic liquid was synthesized through an anion exchange reaction following a previously reported protocol[25] and was stored in a glovebox to avoid water absorption. The PMMA/[EMI][TFSI] solutions and all ion gels were prepared by mixing weighed amounts of the respective polymer and the ionic liquid in CH_2Cl_2 cosolvent. After stirring for 2 h, the mixtures were blown with nitrogen gas for a day to evaporate most of the cosolvent. Finally, the samples were placed in a vacuum oven at 70 °C for 2 days to completely remove the cosolvent. To avoid any effects of moisture, all samples were kept in a vacuum desiccator and were dried in a vacuum oven at 70 °C for a day before any measurements were carried out.

Rheology and Impedance Spectroscopy. Rheological and impedance measurements were conducted on ARES rheometers (Rheometric Scientific), one of which was connected to an Agilent 4284A LCR bridge (TA Instruments), using parallel plate geometry. Depending on the modulus, both 50 and 25 mm diameter plates were employed. For [EMI][TFSI] and samples requiring 50 mm diameter plates for rheology, i.e., gels with 10 wt % polymer, impedance measurements were conducted on different samples using 25 mm stainless steel electrodes. Otherwise, all measurements were performed on the same sample with a gap spacing of ~1 mm. All plates were used as fabricated without further surface treatment. At each temperature, the sample was thermally equilibrated for 15−20 min and the gap was adjusted to compensate for the thermal expansion of the tool set; then the dynamic shear moduli were examined in the linear viscoelastic regime, followed by measurements of complex impedance at a shear frequency of 10 rad/s using an ac signal of 0.1 V amplitude in the electrical frequency range of $20-2 \times 10^6$ Hz. The shear frequency was set to 10 rad/s because the instrument requires that impedance data be recorded at a finite shear frequency. There was no dependence of impedance on shear frequency between 1 and 100 rad/s. Temperatures were controlled to within 0.2 °C of the set points with an environmental control circulator under a nitrogen atmosphere.

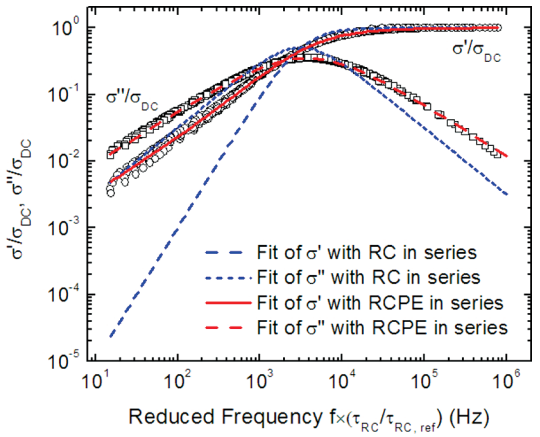

Figure 1. Complex conductivity of SMS/[EMI][TFSI] ion gel with 40 wt % SMS measured over the temperature range of 30−200 °C referenced to 120 °C. The data have been horizontally shifted by $\tau_{RC}/\tau_{RC,120\,°C}$. τ_{RC} corresponds to the maximum in the σ'' vs frequency curve. The vertical shifts are the dc conductivities of the gel at different temperatures.

For [EMI][TFSI] and gels with 10 wt % polymer, impedance measurements were also performed with a homemade cell using a Solartron 1255B frequency response analyzer connected to a Solartron SI 1287 electrochemical interface. Frequency sweeps were conducted from 1 to 10^6 Hz with an ac amplitude of 10 mV. The cell is composed of a Teflon spacer with an inner diameter of 4 mm and a thickness of 2 mm sandwiched between two platinum-coated stainless steel electrodes. Temperatures were controlled to within 0.5 °C of the set points with a thermostated water bath. The samples were thermally equilibrated for 30 min prior to the measurements.

Results and Discussion

Complex Conductivity Spectra. The impedance of the SMS(18−86−18)- and SOS(3−35−3)-based gels were measured over the temperature ranges of 25−200 and 25−160 °C, respectively. Figure 1 displays the normalized complex conductivity spectra (σ' and σ'') of the ion gel with 40 wt % SMS(18−86−18), referenced to 120 °C. The data were horizontally shifted by the ratios of RC time constants at other temperatures (τ_{RC}) to that at the reference temperature ($\tau_{RC,\mathrm{ref}}$). (The RC time constant corresponds to the maximum of the σ'' vs frequency curve which shifts as a function of temperature.) Further discussion of τ_{RC} is deferred until later. In Figure 1, the spectra at different temperatures overlay quite well, indicating that time−temperature superposition (tTS) holds for the gel with 40 wt % SMS(18−86−18). If the stainless steel electrodes are considered to be ideally polarizable within the electrochemical window of [EMI][TFSI], the cell can be represented by a resistor with solution resistance R in series with a capacitor with double-layer capacitance C.[45] Therefore, the total impedance (Z^*) of the system is

$$Z^* = Z' - iZ'' = R + (i\omega C)^{-1} \quad (1)$$

Equivalently, the complex conductivity (σ^*) can be expressed as

$$\sigma^* = \frac{l}{A[R + (i\omega C)^{-1}]} \quad (2)$$

where l is the sample thickness and A is the electrode area. The dc conductivity σ (or solution resistance R) can be obtained from the high-frequency plateau in σ' where the gel is purely resistive. The capacitance C can be calculated from Z'' via eq 1. It is known, however, that the electrical behavior of solid electrode interfaces usually deviates from that of an ideal capacitor in the sense that capacitance is frequency dependent.[46] Two

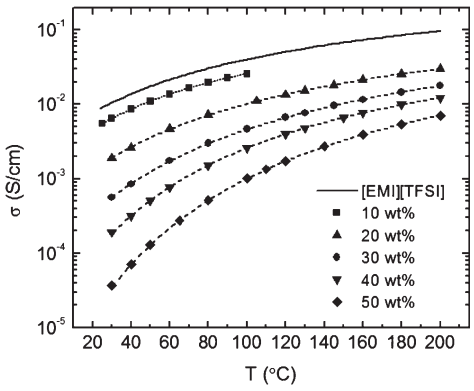

Figure 2. Temperature dependence of ionic conductivity for [EMI][TFSI][52] and the SMS/[EMI][TFSI] ion gels. Dashed lines are best fits using eq 5 (see Table S1 in the Supporting Information for the fitting parameters).

common methods have been utilized to account for this capacitance dispersion phenomenon. One is to calculate the capacitance at a selected frequency of interest, and the other is to model it by a constant phase element (CPE) with impedance $Z_{\mathrm{CPE}} = Q(i\omega)^{-(1-\alpha)}$, where Q and α are positive constants, in order to eliminate the frequency dependence.[47−49] The origin of CPE behavior was first attributed to current density inhomogeneities caused by surface roughness, which depend primarily on a geometric roughness factor. However, later it was reported that this view contradicted measurements performed on rough platinum electrodes, and CPE behavior is mainly due to specific ion adsorption, and possibly broad distributions of time constants associated with these processes.[48,49] Replacing the capacitor with a CPE in the equivalent circuit, the complex conductivity can then be written as

$$\sigma^* = \frac{l}{A[R + Q(i\omega)^{-(1-\alpha)}]} \quad (3)$$

In this case, the CPE is physically equivalent to an RC ladder due to the uneven charging and discharging of the EDLs,[47] and an effective capacitance as defined by eq 1 can be calculated from R and the fitting parameters:

$$C = (R^{\alpha}Q^{-1})^{1/(1-\alpha)} \quad (4)$$

As shown in Figure 1, eq 3 describes the data better than eq 2, especially at low frequencies where the capacitive contribution dominates. Overall, fitting σ^* of all samples with eq 3 yields α values in the range 0.10−0.25, which are comparable to those reported for stainless steel in contact with aqueous solutions.[50,51] For both SMS(18−86−18)- and SOS(3−35−3)-based gels at concentrations below 30 wt % polymer, α decreases with temperature significantly above 40 °C, and tTS fails on the low-frequency side of the spectra (not shown).

Ionic Conductivity. Figure 2 shows the ionic conductivity of the SMS(18−86−18)-based gels. The conductivity of bulk [EMI][TFSI] from a previous report[52] is also plotted for comparison. It has been reported that the temperature dependence of σ for both [EMI][TFSI] and ion gels with chemically cross-linked PMMA follows the Vogel−Fulcher−Tammann (VFT) equation:[25]

$$\sigma = \sigma_0 \exp[-B/(T - T_0)] \quad (5)$$

where σ_0 is a prefactor, B is a constant related to the entropic barrier of conduction, and T_0 is the Vogel temperature. The conductivity data of the gels herein were fit to this equation, as shown by the dashed lines in Figure 2. Not surprisingly, the temperature dependence of σ for the SOS(3−35−3)-based gels follow eq 5 well (see Table S1 in the Supporting

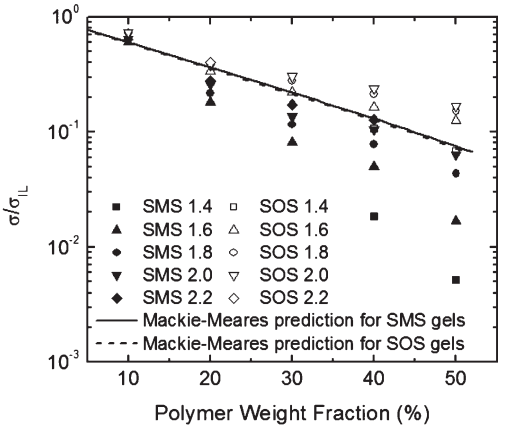

Figure 3. Ionic conductivity normalized with respect to neat [EMI][TFSI] for the ion gels at selected reduced temperatures (T/T_g's).

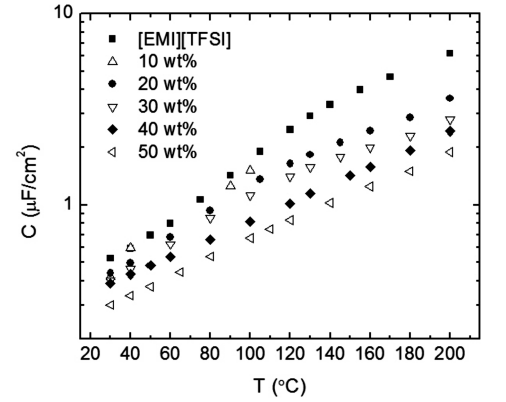

Figure 4. Capacitance calculated from RCPE series circuit fits for [EMI][TFSI] and the SMS/[EMI][TFSI] ion gels.

Information for the fitting parameters). The temperature dependence of σ for the gel with 10 wt % SMS(18−86−18) nearly tracks that of the neat ionic liquid, while σ becomes more temperature dependent as more SMS(18−86−18) is added. This effect is more clearly observed in Figure 3, where the conductivity normalized with respect to neat [EMI][TFSI] is plotted versus polymer weight fraction, at selected reduced temperatures (see Figure S1 and Table S2 in the Supporting Information for the T_g's). The data for SOS(3−35−3)-based gels are also shown as a comparison. At a polymer concentration of 10 wt %, the conductivity is reduced by about 30% for the SOS(3−35−3) gel and by about 36% for the SMS(18−86−18) gel from the pure ionic liquid. These values compare well with previously reported conductivities for both physically cross-linked gels with a PEO midblock (~30%−40% decrease)[32,33] and the ion gel with chemically cross-linked PMMA (~40% decrease).[25] Moreover, despite the huge difference in glass transition temperatures (T_g) and differences in molecular weight and volume fraction of the bridging polymers, the conductivity with addition of 10 wt % SOS(3−35−3) and SMS(18−86−18) is almost the same. These observations are consistent with the expectation that in a moderately dilute polymer solution the relaxation of the polymer chains scales with the solvent viscosity, while the solvent motion is only weakly affected by polymer. As more SMS(18−86−18) is added, the glassy PMMA block (T_g ~ 110 °C)[38] increases the glass transition temperature and broadens the DSC glass transition widths (Figure S1a and Table S2 in the Supporting Information). This brings the measured temperature range closer to the glass transition of the conducting PMMA/[EMI][TFSI] phase at higher SMS(18−86−18) weight fractions, leading to a more temperature-dependent ionic conductivity. On the other hand, since PEO is very flexible (T_g ~ −60 °C),[38] this effect is much weaker and the measured temperature range stays well above the glass transition even with 50 wt % addition of SOS(3−35−3) (Figure S1b and Table S2 in the Supporting Information), which results in much less temperature-dependent ionic conductivity of the SOS(3−35−3)-based gels than the SMS(18−86−18)-based ones.

At a polymer content of 10 wt %, the ionic conductivity is comparable to the prediction of the obstruction model developed by Mackie and Meares (Figure 3).[53] In a hypothetical lattice randomly occupied by equally sized polymer chain segments and solvent molecules, assuming that solvent diffusion occurs through the lattice sites unoccupied by the polymer, the ratio of diffusion coefficient in the gel (D_g) to that of the neat solvent (D_0) can be written as[54]

$$\frac{D_g}{D_0} = \left(\frac{1-\varphi}{1+\varphi}\right)^2 \tag{6}$$

where φ is the polymer volume fraction. Assuming the number density of conducting ions is the same for the gel and the neat solvent, a similar relationship applies to ionic conductivity

$$\frac{\sigma_g}{\sigma_0} = \left(\frac{1-\varphi}{1+\varphi}\right)^2 \tag{7}$$

where σ_g and σ_0 are conductivity of the gel and ionic liquid, respectively. At higher polymer concentrations, the Mackie−Meares prediction qualitatively agrees with σ of the SMS(18−86−18)-based gels at the highest two T/T_g's and that of the SOS(3−35−3)-based gels at the lowest T/T_g. Note that even though the selected reduced temperatures of the SMS and SOS gels are the same, the glass transition ranges of the SMS gels are much wider than the SOS gels (Figure S1 and Table S2 in the Supporting Information). For the SMS(18−86−18)-based gels, the main contributing factor to the conductivity reduction with respect to the neat ionic liquid is the broadened glass transition widths along with the increased T_g's, rather than the simple blockade of conducting paths for the ions. For SOS gels, on the other hand, the experimental conductivity is slightly higher than the prediction of eq 7 at higher reduced temperatures; this may reflect changes in ion number density.

Double-Layer Capacitance. Figure 4 shows the sheet capacitance for [EMI][TFSI] and the SMS(18−86−18)-based gels calculated from the fitting parameters, assuming an equivalent RCPE series circuit. The SOS(3−35−3)-based gels exhibit similar, but slightly higher, capacitance values than those of the SMS(18−86−18)-based ones. The specific capacitance for [EMI][TFSI] can be roughly estimated using the linearized Gouy−Chapman theory:

$$C = \frac{\varepsilon\varepsilon_0}{\lambda} \tag{8}$$

where ε is the relative permittivity, ε_0 is the vacuum permittivity, and λ is the Debye length, which is given by[45]

$$\lambda = \sqrt{\frac{\varepsilon\varepsilon_0 k_B T}{e^2 \sum_i z_i^2 n_i}} \tag{9}$$

where k_B is the Boltzmann constant, e is the magnitude of the charge of an electron, z_i is the charge number of species i, and

n_i is the number density of species i. For [EMI][TFSI] at room temperature, taking $\varepsilon \sim 12$,[55,56] $z_{[EMI]} = z_{[TFSI]} = 1$, and $n_{[EMI]} = n_{[TFSI]} \sim 1.5 \times 10^{21}$ cm^{-3},[25] the calculated Debye length is 0.076 nm and the capacitance is 140 μF/cm^2. This calculated Debye length is clearly unphysical since it is smaller than the ionic radii of the component ions. Measurement of forces normal to ionic liquid/mica interfaces showed that the effective Debye lengths of ionic liquids are on the order of 1−4 nm,[57] which agree with other reported EDL thickness values of around 1 nm for ionic liquids.[58] Thus, more meaningful estimated capacitance values should be about 3−11 μF/cm^2. These are close to those measured at Pt,[59] Au,[60] dropping mercury,[61] and glassy carbon electrodes.[60,61] Recently, it has been reported that the capacitance of EDLs formed at metal/ionic conductor interfaces can be even higher than the prediction based on the Gouy−Chapman theory due to possible binding of the ions to their image charges in the metal.[62] However, the capacitance measured here is smaller ($< 1\,\mu$F/cm^2 at 30 °C) than the Gouy−Chapman prediction. This difference possibly originates from the nature of the stainless steel electrodes and calculating capacitance from fitting over the entire frequency range (20 Hz−2 MHz). The possible effect of the roughness of the electrodes is an important point. Measurements of identical gel samples containing 10 wt % SMS(18−86−18) with evaporated platinum contacts on a different impedance apparatus (described in the Experimental Section) yield $C \sim 6\,\mu$F/cm^2 at 1 Hz at 30 °C. Thus, the method we have chosen to determine capacitance (namely, by fitting the entire frequency range up to 2 MHz using rough electrodes) has suppressed the values of C that one would determine under more "steady state" conditions.

It is evident from Figure 4 that capacitance increases with temperature for both [EMI][TFSI] and the SMS(18−86−18)-based gels. The same trend was observed with the SOS-(3−35−3)-based gels and has been reported for a number of imidazolium-based ionic liquids[63−66] and high-temperature molten salts.[67,68] This contradicts the predictions of the Gouy−Chapman theory since capacitance should decrease with increasing temperature as evidenced by eqs 8 and 9 (the dielectric constant decreases slightly[55] and the Debye length increases with increasing temperature). Monte Carlo simulations based on mixtures comprised solely of charged spheres, on the other hand, successfully predict the measured trend at low reduced temperatures.[69] Even though these simulations aimed to address high-temperature molten salts, they provide insight into the important role of electrostatic interactions in affecting the temperature dependence of capacitance for ionic liquids. While there is no general agreement on the physical origins that account for this trend, possible explanations include reduced interionic interactions and facilitated ion dissociation with increased temperature.[63,65,70]

The double-layer capacitance decreases with increasing polymer content, as shown in Figure 4. This is presumably due to the increased area occupied by polymer chains along the electrode surface and therefore altered structures of the EDLs as more polymers are added. However, this effect does not seem to be very strong, and the reduction in capacitance for a gel with 50 wt % SMS(18−86−18) relative to neat [EMI][TFSI] is within a factor of 3. Nor is the reduction very temperature dependent, in contrast to the ionic conductivity. This is likely because capacitance pertains to the property of the established EDLs along the interface, while ionic conductivity is a measure of charge transport in the bulk, which depends on ion mobilities that are strongly affected by temperature.

***RC* Time Constant.** Shifting σ^* along the frequency axis by the ratio of peak positions of σ'' at different temperatures gives the tTS master curves shown in Figure 1. These peak positions correspond to the product of bulk resistance R and double-layer capacitance C, indicating that the characteristic time (τ_{RC}) of the ionic motion examined in this study relates to the establishment of stable EDLs along the electrolyte/electrode interfaces. Therefore, for electrochemical devices where stable EDLs are needed, the operating frequency is potentially limited by the value of τ_{RC}. Figure 5 shows τ_{RC} calculated at a thickness of 1 mm and an electrode diameter of 25 mm. The opposite temperature and concentration dependences of R and C result in an intermediate dependence of τ_{RC}. However, since both dependences are stronger for R than for C, those of τ_{RC} resemble R more, as shown by the nearly opposite trends of Figures 5 and 3. It is worth noting that the value of R, and thus τ_{RC}, varies linearly with sample thickness and that by reducing the sample thickness into the micrometer range, much smaller relaxation times can be obtained.[71]

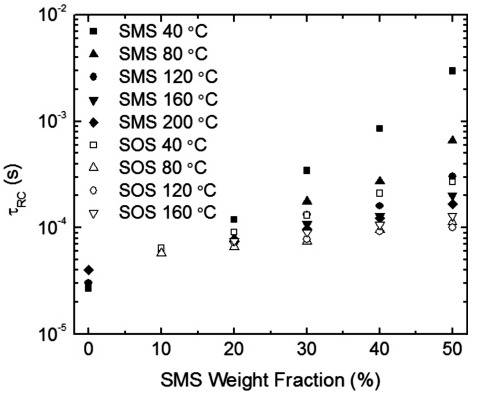

Figure 5. *RC* time constant at a thickness of 1 mm and an electrode diameter of 25 mm for [EMI][TFSI] and the ion gels. C was calculated from RCPE series circuit fits.

Rheology of Ion Gels. Figure 6 shows the dynamic storage (G') and loss (G'') moduli as a function of frequency for the SMS/[EMM][TFSI] ion gel with 10 wt % SMS(18−86−18) over the temperature range 30−200 °C. At each temperature, strain sweeps were conducted first to determine the linear viscoelastic regime. The results are reversible in the sense that the modulus values are independent of whether the measurements are conducted in a heating or a cooling manner. Rubberlike behavior is observed over the entire investigated temperature and frequency ranges, as indicated by $G' > G''$ and the weakly frequency dependent plateaus in G'. Note that in the low-temperature region (30−75 °C) G' is almost independent of temperature at frequencies below 10 rad/s, which is indicative of a network structure that is almost invariant. Increasing the temperature moves a second plateau into the measured frequency window, and by 140 °C two distinct plateaus could be observed. Further increases in temperature reveal the second plateau, as evidenced by the nearly constant G' at low frequencies in the temperature range 160−200 °C. These results are qualitatively similar to those previously reported for SOS/[BMI][PF_6][32] and SOS/[EMI]-[TFSI][34] ion gels. Additionally, it is clear that the plateau modulus decreases with increasing temperature. The plateau modulus of an elastic polymer network (G) can be written as[72]

$$G = \nu k_B T \tag{10}$$

where ν is the number density of network strands. If the structure of the gel does not change, then the modulus should increase with temperature. The opposite observed trend here indicates that the relaxation of the physical cross-links

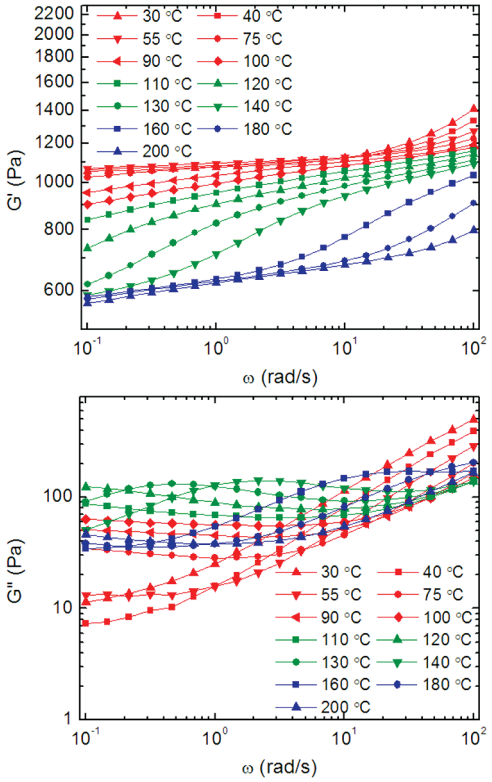

Figure 6. Frequency dependences of dynamic storage and loss moduli for the SMS/[EMI][TFSI] ion gel with 10 wt % SMS(18−86−18).

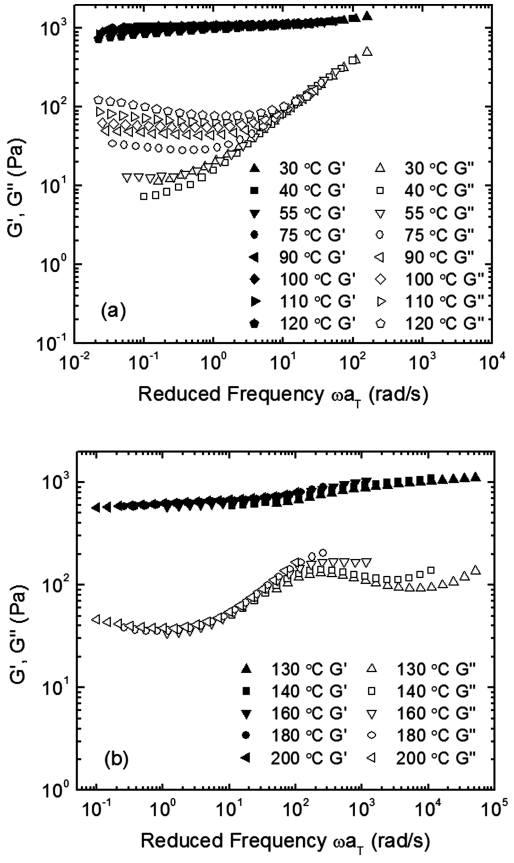

Figure 7. Dynamic storage and loss moduli for SMS/[EMI][TFSI] ion gel with 10 wt % SMS(18−86−18) shifted to (a) 40 °C and (b) 200 °C, corresponding to the fast and slow relaxation modes, respectively.

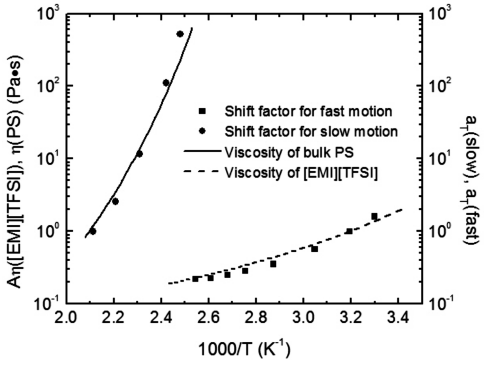

Figure 8. Temperature dependences of the slow and fast relaxation modes of the SMS network in the SMS/[EMI][TFSI] ion gel with 10 wt % SMS(18−86−18). The shift factors were obtained by superposing the fast and slow relaxations in the loss tangent spectrum (Figure 7). The viscosity data of bulk PS and bulk [EMI][TFSI] are presented as a comparison. A vertical shift (A = 51) was applied to the viscosity of [EMI][TFSI] to compare only the temperature dependence. The bulk PS viscosity data were shifted to lower temperatures by 28 K, indicating a reduction in T_g for the micellar PS cores with respect to the bulk PS.

reduces the network stress more than the temperature increase upon heating. Further discussion on the comparison between the measured modulus values and those calculated using eq 10 is deferred until later.

The observation of two plateaus in G' and the reduced plateau modulus with increasing temperature suggest that two relaxation processes are present in the ion gel, as illustrated by the tTS curves in Figure 7. Reasonable superpositions of the moduli were obtained at the high-frequency side of the fast relaxation (Figure 7a) and at the low-frequency side of the slow relaxation (Figure 7b). In the intermediate frequency/temperature range, tTS fails because both relaxations are evident.

To understand the relaxation processes better, the horizontal shift factors (a_T) used to generate the superpositions in Figure 7 are plotted against inverse temperature, as shown in Figure 8. The temperature dependences of the viscosity of neat [EMI][TFSI] and bulk PS taken from refs 52 and 73, respectively, are also shown for comparison. It is evident that a_T of the fast relaxation mode follows the temperature dependence of the [EMI][TFSI] viscosity, while a_T of the slow relaxation mode tracks the temperature dependence of the PS viscosity. This suggests that the fast relaxation corresponds to the motion of the bridging PMMA chains in [EMI][TFSI], which tracks the temperature dependence of the solvent viscosity for this moderately dilute system. The slow relaxation, on the other hand, reflects the motion of the PS chains. In order to dissociate and diffuse into the PMMA/[EMI][TFSI] matrix, the PS chains need to overcome an energy barrier.[74] The value of this barrier depends on the incompatibility χN between PS and [EMI][TFSI], where χ is the Flory−Huggins interaction parameter and N is the degree of polymerization of the PS block.[75] Taking $\chi \sim 0.38$[34] and N = 168 for the SMS gels, the energy barrier is about $64kT$. Therefore, it is highly unlikely that the PS chains would be pulled out from the cross-links. This relaxation reduces the stretching of the bridging PMMA chains and therefore leads to a lowered stress and plateau modulus of the network upon heating. Note that according to eq 10 there should not be a decrease in modulus unless the number of elastically effective strands decreases. However, in the ion gels the "cross-links" are not points, but finite micelles, so passing through the glass transition of these cores is somewhat analogous to allowing the cross-links to become mobile and rearrange to

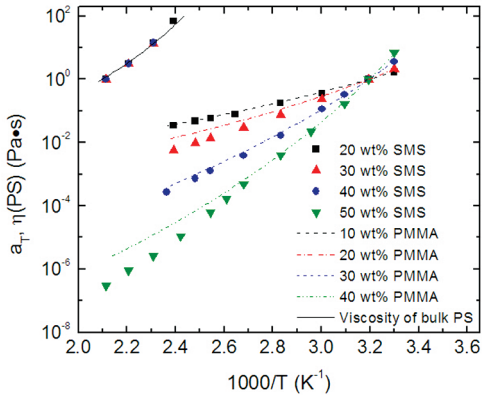

Figure 9. Temperature dependences of the slow and fast relaxation modes of the SMS network in SMS/[EMI][TFSI] ion gels. The viscosity data of bulk PS and the Williams−Landel−Ferry (WLF) fits (see Table S3 in the Supporting Information for the fitting parameters) of shift factors for PMMA/[EMI][TFSI] solutions are presented as comparisons. PMMA concentrations in ion gels with 20, 30, 40, and 50 wt % SMS(18−86−18) are 14, 21, 28, and 36 wt %, respectively. The bulk PS viscosity data were shifted to lower temperatures by 28 K, indicating a reduction in T_g for the micellar PS cores with respect to the bulk PS.

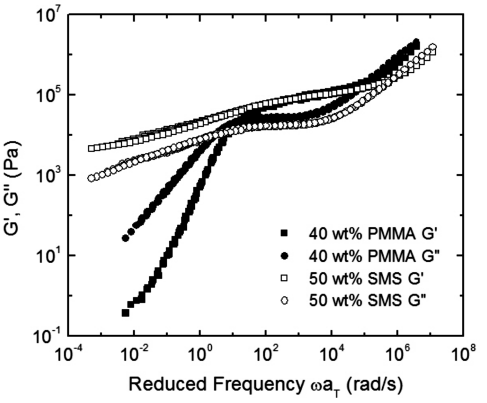

Figure 10. tTS master curves for dynamic storage and loss moduli referenced to 120 °C of PMMA/[EMI][TFSI] solution with 40 wt % PMMA(126)[77] and SMS/[EMI][TFSI] ion gel with 50 wt % SMS(18−86−18).

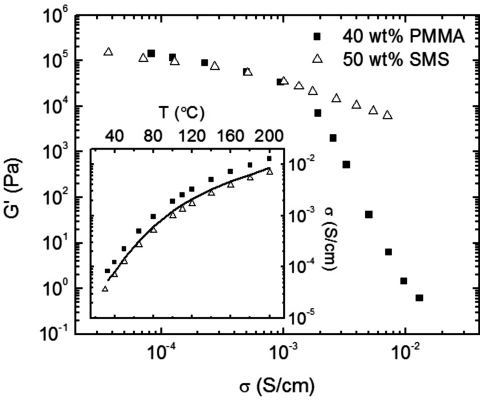

Figure 11. Storage modulus versus ionic conductivity of PMMA/[EMI][TFSI] solution with 40 wt % PMMA(126) and SMS/[EMI]-[TFSI] ion gel with 50 wt % SMS(18−86−18). Inset shows the temperature dependence of the ionic conductivity. Solid line in the inset is calculated conductivity for a hypothetical gel composed of 40 wt % PMMA, 10 wt % PS, and 50 wt % [EMI][TFSI].

reduce the stress. Note also that in Figure 8 the bulk PS (T_g = 95 °C) viscosity data taken from ref 73 were shifted to lower temperatures by 28 K, indicating that the T_g of the PS cores is reduced to about 67 °C. This transition was not observed in the DSC traces (Figure S1 in the Supporting Information), likely due to the very small amount of the cross-linking cores. However, such a reduction in T_g is not surprising.[75,76]

The effect of SMS content on the temperature dependence of the relaxations is illustrated in Figure 9. The shift factors of the slow relaxation for ion gels with 20−40 wt % SMS-(18−86−18) overlap and track the temperature dependence of PS viscosity, as is the case with 10 wt % SMS(18−86−18), whereas a_T of the fast relaxation does not follow the temperature dependence of [EMI][TFSI] viscosity anymore. This is reasonable, since the concentrations of PMMA chains in these gels are no longer in the moderately dilute regime. In these cases, a_T of the fast relaxation (colored symbols in Figure 9) tracks the temperature dependence of a_T of a PMMA/[EMI][TFSI] solution with a similar PMMA(126) concentration to that in the gel (dashed lines in Figure 9).[77] This supports the speculation that the fast relaxation is the motion of PMMA chains in [EMI][TFSI].

For the ion gel with 50 wt % SMS(18−86−18) (36 wt % PMMA), it can be seen from Figure 9 that a_T of this gel follows the temperature dependence of a_T of the homopolymer solution with 40 wt % PMMA(126) below 140 °C. Even more striking than the similarity of a_T is the comparable relaxation times, as evidenced by the near-overlap of moduli at high frequencies (> 10 rad/s) shown in Figure 10. This confirms the notion that the PMMA middle blocks in the gel relax in a way similar to free PMMA coils in the solution. The small disparity in moduli is probably due to differences in PMMA concentration (36 wt % in the gel versus 40 wt % in the solution) and molecular weight (Table 1). This similarity in moduli at high frequencies has also been observed for the ion gel with 40 wt % SMS(18−86−18) (28 wt % PMMA) versus the homopolymer solution with 30 wt % PMMA(126) (Figure S2 in the Supporting Information).

Returning to the comparison of the ion gel and homopolymer solution with the highest polymer concentrations, below 140 °C, one would expect similar ion transport behaviors owing to the similarity of PMMA relaxations. Indeed, the ionic conductivity of the gel compares well with that of the PMMA solution, as illustrated in the left portion of Figure 11 ($\sigma < 10^{-3}$ S/cm). Above 140 °C, the conductivity of the gel remains comparable to the homopolymer solution, as shown in the right portion of Figure 11 ($\sigma > 10^{-3}$ S/cm), but the modulus of the homopolymer solution naturally collapses. In this temperature range the ionic conductivity is completely decoupled from mechanical stability, which is reasonable since the conductivity relies on the conducting phase (PMMA/[EMI][TFSI]) while the modulus is influenced by the presence of the insulating phase (PS).

Over the whole temperature range, the conductivity of the gel with 50 wt % SMS is shifted to lower values by a certain amount from the homopolymer solution with 40 wt % PMMA(126), as evidenced in the inset of Figure 11. The amount of shift agrees qualitatively with the prediction based on Mackie−Meares model, taking the solution with 40 wt % PMMA(126) as the reference and subtracting 10 wt % PS as the obstruction. The slight overestimation based on this hypothetical gel can be ascribed to the difference in the amount of the insulating PS phase, which is 14 wt % in the actual gel with 50 wt % SMS(18−86−18). Therefore, conductivity is really only affected by the concentration of polymers in the conducting phase and the space occupied by the insulating phase, regardless of whether the system forms a gel or not.

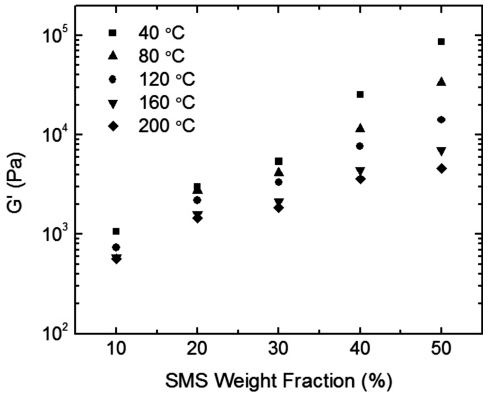

Figure 12. Storage modulus at 0.1 rad/s for the SMS/[EMI][TFSI] ion gels.

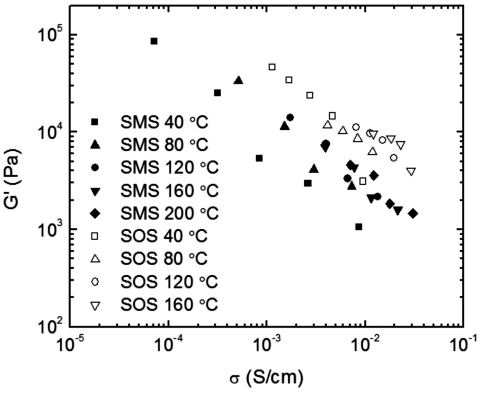

Figure 13. Storage modulus at 0.1 rad/s versus ionic conductivity for SMS/[EMI][TFSI] and SOS/[EMI][TFSI] ion gels with SMS-(18−86−18) and SOS(3−35−3) concentrations of 10, 20, 30, 40, and 50 wt %.

As mentioned before, the entropic elasticity based on eq 10 predicts increasing modulus with temperature, whereas the measured values decrease for the gel with 10 wt % SMS-(18−86−18) due to faster release of stress by the relaxation of the PS chains. This trend holds for gels with higher SMS concentrations as well, as displayed in Figure 12. For an ideal gel where every midblock is effective, $\nu = cN_A/M_x$, where c is the concentration of the block copolymer in w/v, N_A is Avogadro's number, and M_x is the molecular weight between cross-links. Therefore, eq 10 can be written as

$$G = \frac{cfRT}{M_x} \tag{11}$$

where f is the fraction of bridging or effective middle blocks inside the copolymer and R is the ideal gas constant. Assuming all PMMA chains bridge two cross-linking cores instead of looping back to the same one ($f = 1$), and the molecular weight between cross-linking points is simply that of the entire PMMA chain ($M_x = M_{n,PMMA}$), the modulus values calculated from eq 11 at 40 °C are 3.2, 6.1, 8.9, 12, and 14 kPa for SMS/[EMI][TFSI] ion gels with 10, 20, 30, 40, and 50 wt % SMS(18−86−18), respectively. Comparing these values with the measured ones in Figure 12, it is clear that eq 11 overpredicts the effect of SMS concentration on network modulus for gels with 10−30 wt % SMS(18−86−18) but underestimates the modulus for gels with 40 and 50 wt % SMS(18−86−18). This is not surprising due to the two crude assumptions made above. Given the entanglement molecular weight (M_e) of 10 kDa for PMMA at 140 °C[78] and the PMMA weight fractions in the gels, the effective M_e of PMMA in the gels are 143, 71, 47, 36, and 28 kDa from low to high SMS content. Since $M_e < M_{n,PMMA}$ for gels with 30−50 wt % SMS(18−86−18), the assumption $M_x = M_{n,PMMA}$ should be replaced with $M_x = M_e$. This is consistent with the observation of similar moduli at high frequencies for gels and solutions with the highest two polymer concentrations (Figure 10 and Figure S2 in the Supporting Information) and explains the underestimation of modulus for gels with 40 and 50 wt % SMS(18−86−18). For gels with 10 and 20 wt % SMS(18−86−18), where no PMMA entanglements are present, the overestimation of modulus is due to ineffective loops which renders the actual value of f less than unity. Comparison of the calculated values to the measured ones yields bridging fractions of 0.34 and 0.48 for gels with 10 and 20 wt % SMS(18−86−18), respectively, which are comparable to previously reported gels.[32,79] For the gel with 30 wt % SMS(18−86−18), the effects of light entanglement and ineffective loops counteract each other, resulting in slightly lower measured modulus compared to the prediction of eq 11.

Correlation of Modulus with Conductivity. Figure 13 summarizes the storage modulus and ionic conductivity for SMS(18−86−18)- and SOS(3−35−3)-based ion gels in the temperature range 40−200 °C and the polymer concentration range 10−50 wt %. Both parameters extend several orders of magnitude. Obviously, the accessible modulus and conductivity windows can be extended even further by the choice of different ionic liquids. Thus, for a given electrochemical application, one could design appropriate gels to meet the specific requirements by tuning the identity and molecular weight of the blocks, the polymer content, and the ionic liquid. For a given ionic liquid, in this case [EMI][TFSI], the elastic modulus of the gels is roughly inversely proportional to the ionic conductivity. Therefore, for certain applications where gels are required to be both highly conductive and mechanically robust, e.g. electromechanical actuators, other strategies will need to be developed for the system to lie above the diagonal in Figure 13. On the whole, the SOS(3−35−3)-based gels are more conductive and exhibit higher modulus values than the SMS(18−86−18)-based gels at the same polymer concentration. The higher modulus of the SOS gels is mainly due to the lower molecular weight of the O blocks (eq 11). In general, for gels based on SMS and SOS with the same block lengths and concentration, the SOS gels are expected to exhibit conductivity and modulus values greater than or equal to the SMS gels. In practice, other design criteria specific to the target application will need to be considered to determine which triblock to choose.

Conclusions

We have examined the electrical and viscoelastic properties of ion gels based on SMS(18−86−18) and SOS(3−35−3) triblock copolymers and the ionic liquid [EMI][TFSI] over wide temperature and composition ranges. The gels are thermally stable up to at least 200 and 160 °C, respectively, with conductivity and modulus extending several orders of magnitude. This provides evidence for the tunability of such block copolymer-based ion gels.

The response of the ion gels to ac electric fields below 1 MHz is similar to an RCPE series circuit, with a characteristic time corresponding to the establishment of stable EDLs. For concentrated SMS gels, the R or σ values are strongly affected by the glassy midblocks because they represent ion transport in the bulk, while C is not affected as much due to the nature of the gel/electrode interfaces. For SOS gels, the σ values are higher and

much less dependent on either temperature or concentration. The opposite temperature and concentration dependences of R and C yield intermediate dependences for τ_{RC}.

Under oscillatory mechanical shear, two relaxation modes are observed in the SMS ion gels. The fast mode is associated with the relaxation of the midblocks in the ionic liquid, which is remarkably similar to that of free chains in homopolymer solutions. The slow mode is related to the motion of the end-blocks within their micellar cores. Comparison of conductivity and modulus between the gel and the solution with the highest polymer concentrations studied reveals that ion transport and mechanical stability can be decoupled.

Acknowledgment. This work was supported by the National Science Foundation through the MRSEC program at the University of Minnesota, Award DMR-0819885. We thank Professor Philippe Buhlmann for access to his impedance spectroscopy equipment.

Supporting Information Available: VFT fitting parameters of conductivity for the SMS/[EMI][TFSI] and SOS/[EMI]-[TFSI] ion gels, DSC characterization of [EMI][TFSI] and the ion gels, WLF fitting parameters of shift factors for PMMA/[EMI]-[TFSI] solutions, and rheology master curves for SMS/[EMI]-[TFSI] ion gel with 40 wt % SMS(18−86−18) and PMMA/[EMI][TFSI] solution with 30 wt % PMMA(126). This material is available free of charge via the Internet at http://pubs.acs.org.

References and Notes

(1) Welton, T. *Chem. Rev.* **1999**, *99*, 2071–2083.
(2) Dyson, P. J.; Geldbach, T. J. *Electrochem. Soc. Interface* **2007**, *16*, 50–53.
(3) Pandey, S. *Anal. Chim. Acta* **2006**, *556*, 38–45.
(4) Galinski, M.; Lewandowski, A.; Stepniak, I. *Electrochim. Acta* **2006**, *51*, 5567–5580.
(5) Tsada, T.; Hussey, C. L. *Electrochem. Soc. Interface* **2007**, *16*, 42–49.
(6) MacFarlane, D. R.; Forsyth, M.; Howlett, P. C.; Pringle, J. M.; Sun, J.; Annat, G.; Neil, W.; Izgorodina, E. I. *Acc. Chem. Res.* **2007**, *40*, 1165–1173.
(7) Wasserscheid, P.; Welton, T. *Ionic Liquids in Synthesis*, 2nd ed.; Wiley-VCH: Weinheim, Germany, 2008.
(8) Sangoro, J. R.; Serghei, A.; Naumov, S.; Galvosas, P.; Kaerger, J.; Wespe, C.; Bordusa, F.; Kremer, F. *Phys. Rev. E* **2008**, *77*, 051202/1–051202/4.
(9) Fullerton-Shirey, S. K.; Maranas, J. K. *Macromolecules* **2009**, *42*, 2142–2156.
(10) Hanabusa, K.; Fukui, H.; Suzuki, M.; Shirai, H. *Langmuir* **2005**, *21*, 10383–10390.
(11) Ueno, K.; Hata, K.; Katakabe, T.; Kondoh, M.; Watanabe, M. *J. Phys. Chem. B* **2008**, *112*, 9013–9019.
(12) Ueki, T.; Watanabe, M. *Macromolecules* **2008**, *41*, 3739–3749.
(13) Lodge, T. P. *Science* **2008**, *321*, 50–51.
(14) Tang, J.; Tang, H.; Sun, W.; Plancher, H.; Radosz, M.; Shen, Y. *Chem. Commun.* **2005**, *26*, 3325–3327.
(15) Shin, J.-H.; Henderson, W. A.; Passerini, S. *J. Electrochem. Soc.* **2005**, *152*, A978–A983.
(16) Christie, A. M.; Lilley, S. J.; Staunton, E.; Andreev, Y. G.; Bruce, P. G. *Nature* **2005**, *433*, 50–53.
(17) Lu, W.; Fadeev, A. G.; Qi, B.; Smela, E.; Mattes, B. R.; Ding, J.; Spinks, G. M.; Mazurkiewicz, J.; Zhou, D.; Wallace, G. G.; MacFarlane, D. R.; Forsyth, S. A.; Forsyth, M. *Science* **2002**, *297*, 983–987.
(18) Ding, J.; Zhou, D.; Spinks, G.; Wallace, G.; Forsyth, S.; Forsyth, M.; MacFarlane, D. *Chem. Mater.* **2003**, *15*, 2392–2398.
(19) Lee, J.; Panzer, M. J.; He, Y.; Lodge, T. P.; Frisbie, C. D. *J. Am. Chem. Soc.* **2007**, *129*, 4532–4533.
(20) Cho, J. H.; Lee, J.; He, Y.; Kim, B. S.; Lodge, T. P.; Frisbie, C. D. *Adv. Mater.* **2008**, *20*, 686–690.
(21) Cho, J. H.; Lee, J.; Xia, Y.; Kim, B.; He, Y.; Renn, M. J.; Lodge, T. P.; Frisbie, C. D. *Nature Mater.* **2008**, *7*, 900–906.
(22) Lee, J.; Kaake, L. G.; Cho, J. H.; Zhu, X.-Y.; Lodge, T. P.; Frisbie, C. D. *J. Phys. Chem. C* **2009**, *113*, 8972–8981.
(23) Xia, Y.; Cho, J.; Paulsen, B.; Frisbie, C. D.; Renn, M. J. *Appl. Phys. Lett.* **2009**, *94*, 013304/1–013304/3.
(24) Lee, S. W.; Lee, H. J.; Choi, J. H.; Koh, W. G.; Myoung, J. M.; Hur, J. H.; Park, J. J.; Cho, J. H.; Jeong, U. *Nano Lett.* **2010**, *10*, 347–351.
(25) Susan, M. A. B. H.; Kaneko, T.; Noda, A.; Watanabe, M. *J. Am. Chem. Soc.* **2005**, *127*, 4976–4983.
(26) Seki, S.; Susan, M. A. B. H.; Kaneko, T.; Tokuda, H.; Noda, A.; Watanabe, M. *J. Phys. Chem. B* **2005**, *109*, 3886–3892.
(27) Klingshirn, M. A.; Spear, S. K.; Subramanian, R.; Holbrey, J. D.; Huddleston, J. G.; Rogers, R. D. *Chem. Mater.* **2004**, *16*, 3091–3097.
(28) Neouze, M.-A.; Le Bideau, J.; Gaveau, P.; Bellayer, S.; Vioux, A. *Chem. Mater.* **2006**, *18*, 3931–3936.
(29) Matsumoto, K.; Endo, T. *Macromolecules* **2008**, *41*, 6981–6986.
(30) Matsumoto, K.; Endo, T. *Macromolecules* **2009**, *42*, 4580–4584.
(31) Jana, S.; Parthiban, A.; Chai, C. L. L. *Chem. Commun.* **2010**, *46*, 1488–1490.
(32) He, Y.; Boswell, P. G.; Buehlmann, P.; Lodge, T. P. *J. Phys. Chem. B* **2007**, *111*, 4645–4652.
(33) He, Y.; Lodge, T. P. *Chem. Commun.* **2007**, 2732–2734.
(34) He, Y.; Lodge, T. P. *Macromolecules* **2008**, *41*, 167–174.
(35) Noro, A.; Matsushita, Y.; Lodge, T. P. *Macromolecules* **2008**, *41*, 5839–5844.
(36) Noro, A.; Matsushita, Y.; Lodge, T. P. *Macromolecules* **2009**, *42*, 5802–5810.
(37) Agrawal, R. C.; Pandey, G. P. *J. Phys. D: Appl. Phys.* **2008**, *41*, 223001/1–223001/18.
(38) Brandrup, J.; Immergut, E. H.; Grulke, E. A. *Polymer Handbook*, 4th ed.; Wiley-Interscience: New York, 1999.
(39) Lai, J. T.; Filla, D.; Shea, R. *Macromolecules* **2002**, *35*, 6754–6756.
(40) Matyjaszewski, K.; Xia, J. *Chem. Rev.* **2001**, *101*, 2921–2990.
(41) Patten, T. E.; Xia, J.; Abernathy, T.; Matyjaszewski, K. *Science* **1996**, *272*, 866–868.
(42) Xia, J.; Matyjaszewski, K. *Macromolecules* **1997**, *30*, 7697–7700.
(43) Shipp, D. A.; Wang, J.-L.; Matyjaszewski, K. *Macromolecules* **1998**, *31*, 8005–8008.
(44) Zeroni, I.; Ozair, S.; Lodge, T. P. *Macromolecules* **2008**, *41*, 5033–5041.
(45) Bard, A. J.; Faulkner, L. R. *Electrochemical Methods: Fundamentals and Applications*, 2nd ed.; Wiley: New York, 2001.
(46) De Levie, R. *Electrochim. Acta* **1965**, *10*, 113–130.
(47) Brug, G. J.; Van den Eeden, A. L. G.; Sluyters-Rehbach, M.; Sluyters, J. H. *J. Electroanal. Chem.* **1984**, *176*, 275–295.
(48) Pajkossy, T. *J. Electroanal. Chem.* **1994**, *364*, 111–125.
(49) Pajkossy, T. *Solid State Ionics* **2005**, *176*, 1997–2003.
(50) Huang, V. M.-W.; Vivier, V.; Frateur, I.; Orazem, M. E.; Tribollet, B. *J. Electrochem. Soc.* **2007**, *154*, C89–C98.
(51) Bou-Saleh, Z.; Shahryari, A.; Omanovic, S. *Thin Solid Films* **2007**, *515*, 4727–4737.
(52) Tokuda, H.; Ishii, K.; Susan, M. A. B. H.; Watanabe, M. *J. Phys. Chem. B* **2005**, *109*, 6103–6110.
(53) Mackie, J. S.; Meares, P. *Proc. R. Soc. London* **1955**, *A232*, 498–509.
(54) Amsden, B. *Macromolecules* **1998**, *31*, 8382–8395.
(55) Krossing, I.; Slattery, J. M.; Daguenet, C.; Dyson, P. J.; Oleinikova, A.; Weingaertner, H. *J. Am. Chem. Soc.* **2006**, *128*, 13427–13434.
(56) Izgorodina, E. I.; Forsyth, M.; MacFarlane, D. R. *Phys. Chem. Chem. Phys.* **2009**, *11*, 2452–2458.
(57) Min, Y.; Akbulut, M.; Sangoro, J. R.; Kremer, F.; Prud'homme, R. K.; Israelachvili, J. *J. Phys. Chem. C* **2009**, *113*, 16445–16449.
(58) Fedorov, M. V.; Kornyshev, A. A. *Electrochim. Acta* **2008**, *53*, 6835–6840.
(59) Drueschler, M.; Huber, B.; Passerini, S.; Roling, B. *J. Phys. Chem. C* **2010**, *114*, 3614–3617.
(60) Alam, M. T.; Islam, Md. M.; Okajima, T.; Ohsaka, T. *J. Phys. Chem. C* **2008**, *112*, 16600–16608.
(61) Nanjundiah, C.; McDevitt, S. F.; Koch, V. R. *J. Electrochem. Soc.* **1997**, *144*, 3392–3397.
(62) Skinner, B.; Loth, M. S.; Shklovskii, B. I. *Phys. Rev. Lett.* **2010**, *104*, 128302/1–128302/4.
(63) Zistler, M.; Wachter, P.; Schreiner, C.; Fleischmann, M.; Gerhard, D.; Wasserscheid, P.; Hinsch, A.; Gores, H. J. *J. Electrochem. Soc.* **2007**, *154*, B925–B930.
(64) Lockett, V.; Sedev, R.; Ralston, J.; Horne, M.; Rodopoulos, T. *J. Phys. Chem. C* **2008**, *112*, 7486–7495.
(65) Silva, F.; Gomes, C.; Figueiredo, M.; Costa, R.; Martins, A.; Pereira, C. M. *J. Electroanal. Chem.* **2008**, *622*, 153–160.

(66) Costa, R.; Pereira, C. M.; Silva, F. *Phys. Chem. Chem. Phys.* **2010**, in press .
(67) Ukshe, E. A.; Bukun, N. G.; Leikis, D. I.; Frumkin, A. N. *Electrochim. Acta* **1964**, *9*, 431–439.
(68) Devanathan, M. A. V.; Tilak, B. V. K. S. R. A. *Chem. Rev.* **1965**, *65*, 635–684.
(69) Boda, D.; Henderson, D.; Chan, K.-Y. *J. Chem. Phys.* **1999**, *110*, 5346–5350.
(70) Holovko, M.; Kapko, V.; Henderson, D.; Boda, D. *Chem. Phys. Lett.* **2001**, *341*, 363–368.
(71) Lee, K.-H.; Zhang, S.; Lodge, T. P.; Frisbie, C. D. Submitted to *J. Phys. Chem. B*.
(72) Hiemenz, P. C.; Lodge, T. P. *Polymer Chemistry*, 2nd ed.; CRC Press: New York, 2007.
(73) Chapman, B. R.; Hamersky, M. W.; Milhaupt, J. M.; Kostelecky, C.; Lodge, T. P.; von Meerwall, E. D.; Smith, S. D. *Macromolecules* **1998**, *31*, 4562–4573.
(74) Tanaka, F.; Edwards, S. F. *Macromolecules* **1992**, *25*, 1516–1523.
(75) Choi, S.-H.; Bates, F. S.; Lodge, T. P. *J. Phys. Chem. B* **2009**, *113*, 13840–13848.
(76) Lai, C.; Russel, W. B.; Register, R. A. *Macromolecules* **2002**, *35*, 841–849.
(77) Mok, M.; Liu, X.; Bai, Z.; Lei, Y.; Lodge, T. P. Submitted to *Macromolecules*.
(78) Fetters, L. J.; Lohse, D. J.; Richter, D.; Witten, T. A.; Zirkel, A. *Macromolecules* **1994**, *27*, 4639–4647.
(79) Annable, T.; Buscall, R.; Ettelaie, R.; Whittlestone, D. *J. Rheol.* **1993**, *37*, 695–726.